Electronic Supplementary Material (ESI) for Chemical Communications.

Supporting Information

Core-shell nano-FeS_2@N-doped graphene as advanced cathode material for rechargeable Li-ion batteries

Rui Tan†, Jinlong Yang†, Jiangtao Hu†, Kai Wang, Yan Zhao and Feng Pan*

School of Advanced Materials, Peking University Shenzhen Graduate School,
Shenzhen 518055, People's Republic of China.

†These authors contributed equally to this work.

*Corresponding author: panfeng@pkusz.edu.cn

Experimental section

Synthesis of N-doped pyrite FeS_2@ like graphene materials (FeS_2@N-graphene)

Based on our former work in our group the γ-Fe_2O_3@graphene can be prepared by commercial Prussion Blue (PB) and glucose. Briefly, PB (0.1 g) and glucose (0.1 g) were dispersed in distilled water and ethanol and then were grinding in mortar. The mixture was dried at 80 °C in the air dry oven. Hereafter, the dried mixture was put in the tube oven at 650 °C for 10 hours, in which the PB decomposed and nano-Fe with Fe_xC formed during the procedure. Cooling down to the room temperature, Fe_xC was separated to nano-Fe and thin layer carbon. After exposed in the air, composites were oxided by O_2 by a spontaneous combustion to transfer to γ-Fe_2O_3@graphene.

For synthesis of FeS_2@N-graphene, γ-Fe_2O_3@graphene (0.1g) and sulfur (0.1g) were mixing in the mortar and then sealed at glass tubes whose diameter is 1 cm and length is about 10 cm. All the tubes were calcined at the muffle furnace at 650 °C for 2 hours. Then cool the tubes down to the room temperature and break them to obtain the product. The prepared materials were put into a argon filled tube oven to remove the sulfur on the surface at 300 °C for several hours. Then the last product was obtained. (shown in **Fig. 1a**)

Preparation of polymer electrolytes

The LiTFSI/DOL/DME/$LiNO_3$ electrolyte was composed of 1M LiTFSI and 0.3 M $LiNO_3$ which are dissolved in the 1,3-dioxolane (DOl) and 1,2-dimethoxyethane (DME) solution (1:1 volume ratio).

Preparation of the half cells

For fabricating the cathode, FeS_2@N-graphene, carbon black (super-p) and PTFE were mixing in the isopropanol, in which the weight ratio of FeS_2@N-graphene, carbon black (super-p) and PTFE is 70: 20: 10. While the isopropanol gasified, the mixture resulted into the cathode plate, in which the average density of active materials (FeS_2@N-graphene) is 1.43 mg cm^{-2}. The 2032 coin cells were assembled by the above cathode plates, lithium metal anodes and electrolytes in an argon filled glove box.

Material characterization and instruments

The X-ray diffraction (XRD) patterns of FeS_2@N-graphene was collected from a Bruker D8 Advance diffractometer equipped with Cu-Kα radiation (λ=1.5418 Å) at room temperature from 20° to 90° (The step size is $1.15^{\circ}min^{-1}$). The thermal stability was studied by thermogravimetric analysis (TG) carried out on a TGA/DSC1 system. The morphologies and elements distribution of FeS_2@N-graphene were observed by a scanning electron microscope (ZEISS Supra 55, Oxford X-Max 20, 20 kV) and the thin carbon layers attached to the FeS_2 were observed by high-resolution transmission electron microscopy (HRTEM, JEM-100F, 200 kV). The nitrogen element was doped in mixture, which is further demonstrated by X-ray photoelectron spectroscopy (XPS, Thermo Fisher, ESCALAB 250X). The current-voltage curves were obtained by electrochemical workstation (CHI 604E). The electrochemical characteristics of cells were performed on a Land instrument (Wuhan Land electronic Co., Ltd. China) with tests using cut-off voltages of 1.0 V (discharge) and 3.0 V (charge).

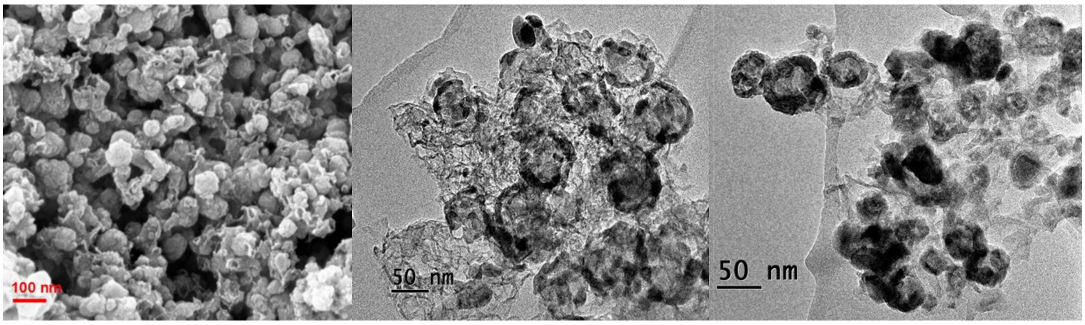

Fig. S1 SEM and TEM images of the intermediate γ-Fe_2O_3. The average size of γ-Fe_2O_3 is 50~100 nm andγ-Fe_2O_3 are tightly connected by thin carbon layers.

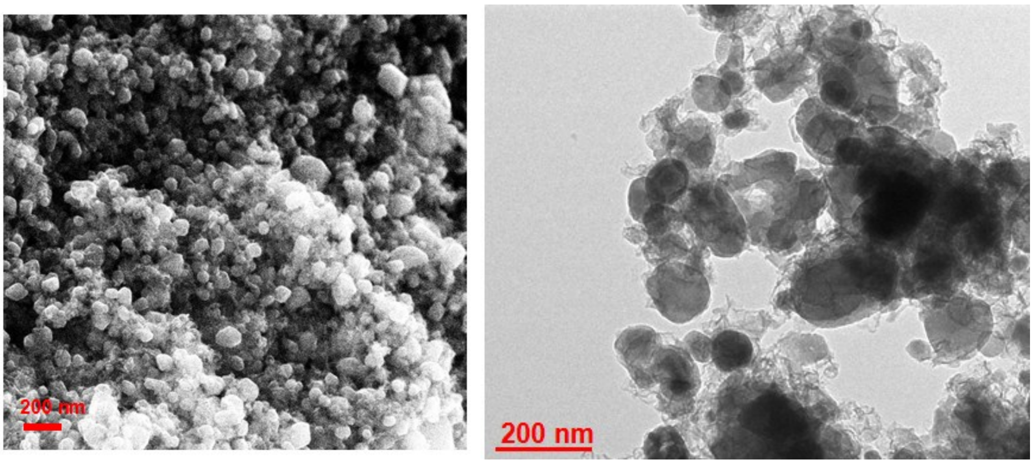

Fig.S2 SEM and TEM images of FeS_2@N-graphene. The second particles of FeS_2@N-graphene and thin carbon layers were shown.

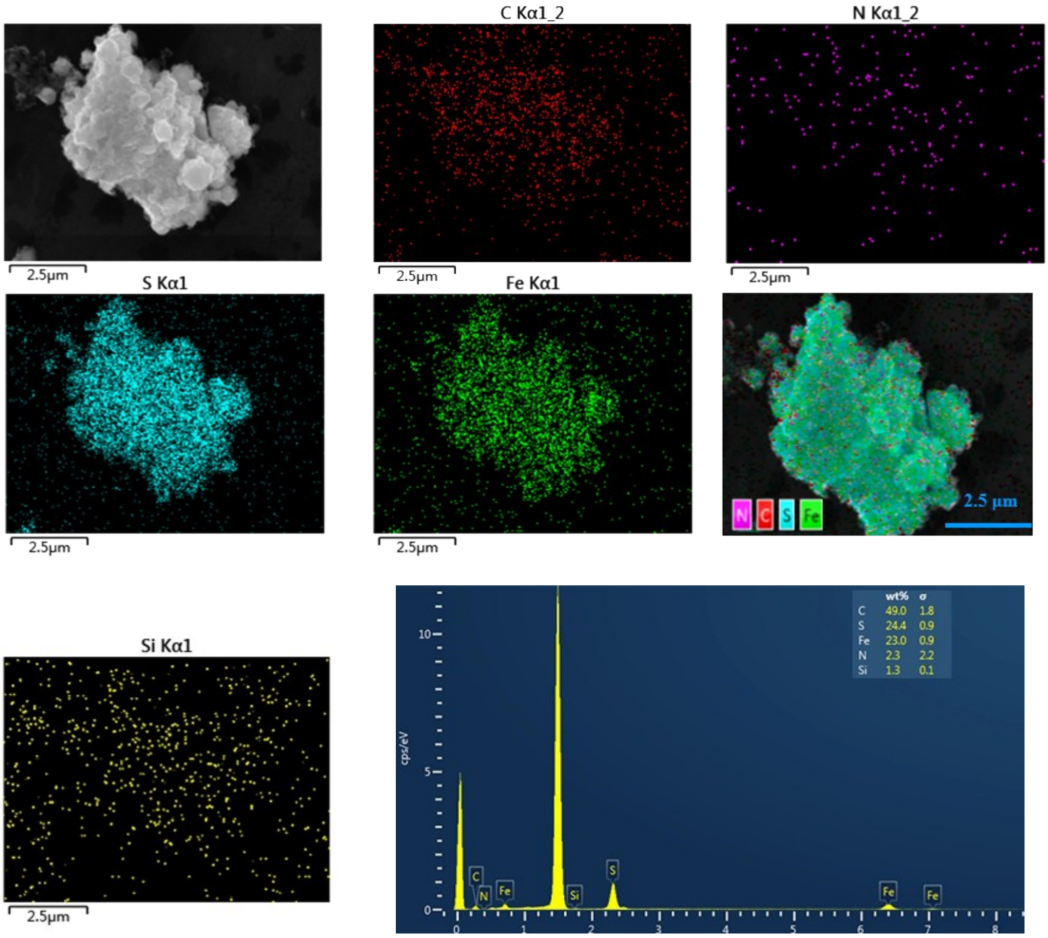

	wt%	σ
C	49.0	1.8
S	24.4	0.9
Fe	23.0	0.9
N	2.3	2.2
Si	1.3	0.1

Fig. S3 EDX images of FeS_2@N-graphene (C, N, S, Fe, Si).

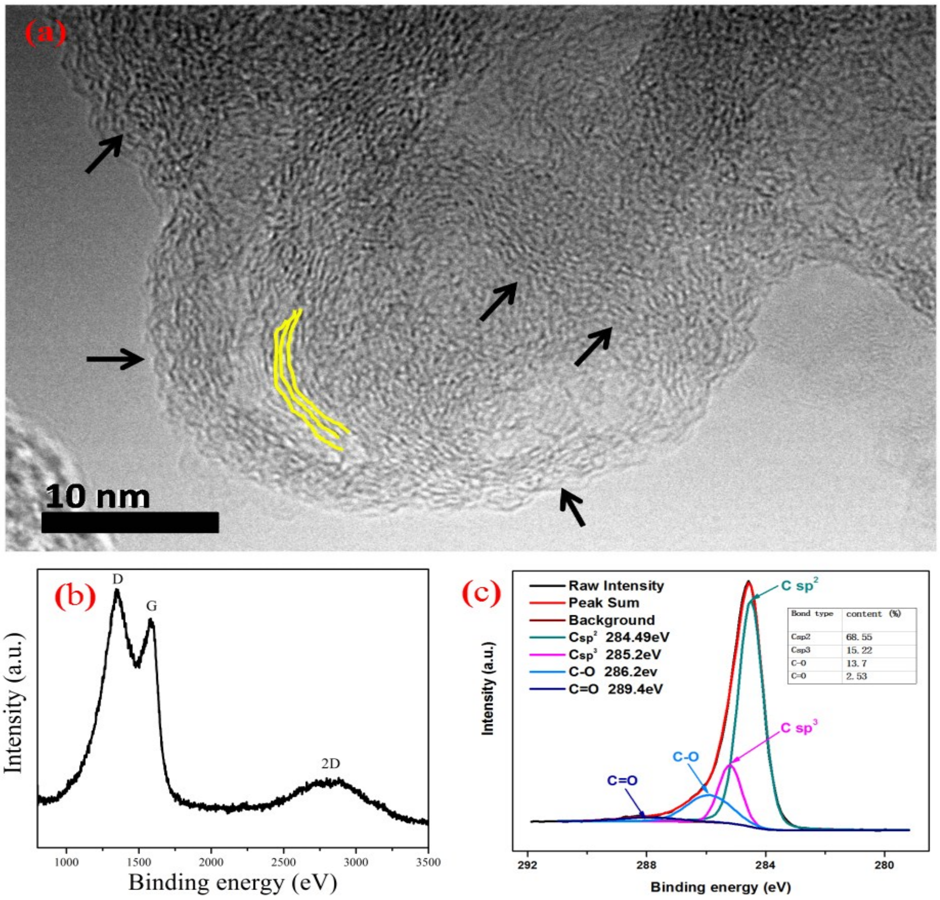

Fig. S4 Characteristics of the graphene shells: (a) high revolution TEM image of the single graphene shell, (b) Raman image , (c) C_{1s} XPS spectra of FeS_2@N-graphene.

HRTEM, Raman and XPS are both used to describe the characteristics of the carbon shells.

The composite materials were put into the high concentration of sulfuric acid solution, after stirring 12 h with the condition of 80 ℃, the C-shell was obtained. HRTEM images (**Fig. R4a**) shows that a large number of graphene layers (the yellow lines and the direction parts of the arrows) are observed. In addition, the 2D peak at 2700 cm^{-1} in Raman spectrum (**Fig. R4b**) is sensitive to the number of graphene layer, which belong to characteristic peak of graphene. In addition, the binding energies at C1s in XPS (**Fig. R4c**) shows high content (68.55%) of sp^2-carbon, indicating a high degree of graphitization. Therefore, HRTEM image, Raman and XPS spectra demonstrate that the coating layer is graphene shell.

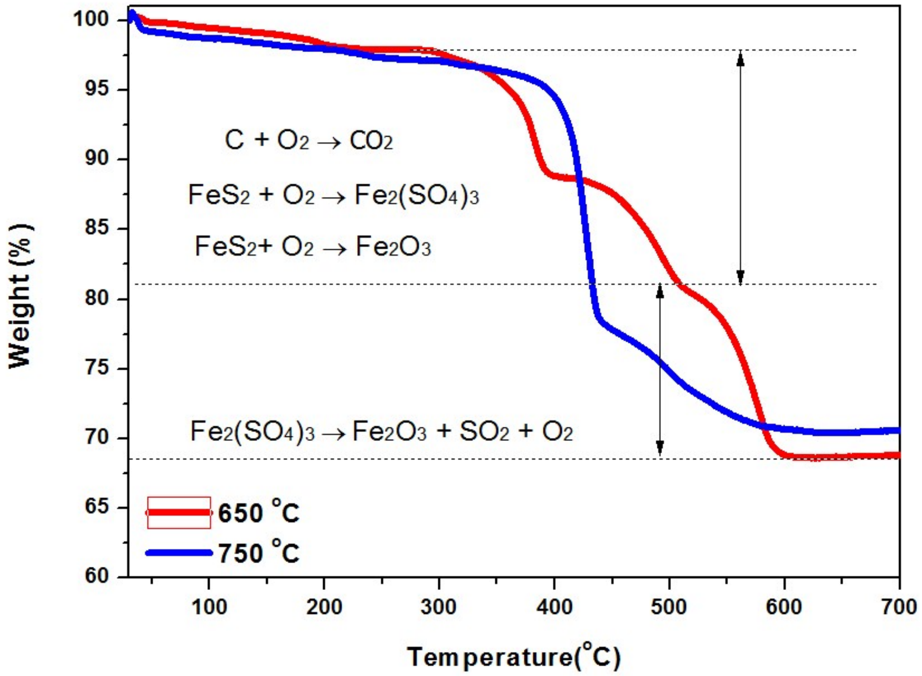

Fig. S5 TG curves of FeS_2@N-graphene at 650 and 750 ^oC.

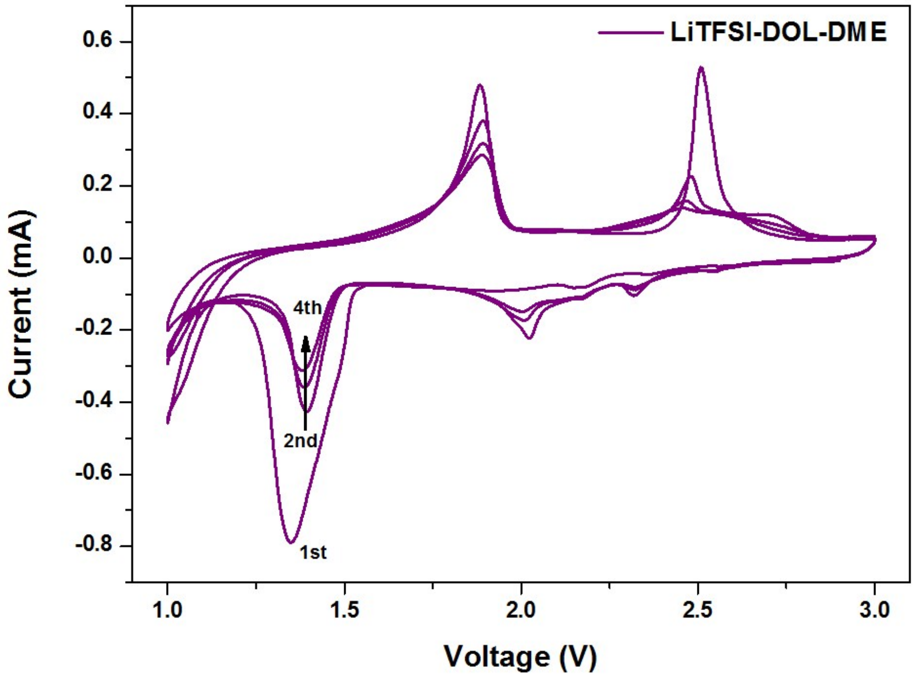

Fig.S6 First four C-V cycles of FeS_2@N-graphene at cells without $LiNO_3$ (the scanning rate is 0.2 mV/s from 1.0 to 3.0 V).

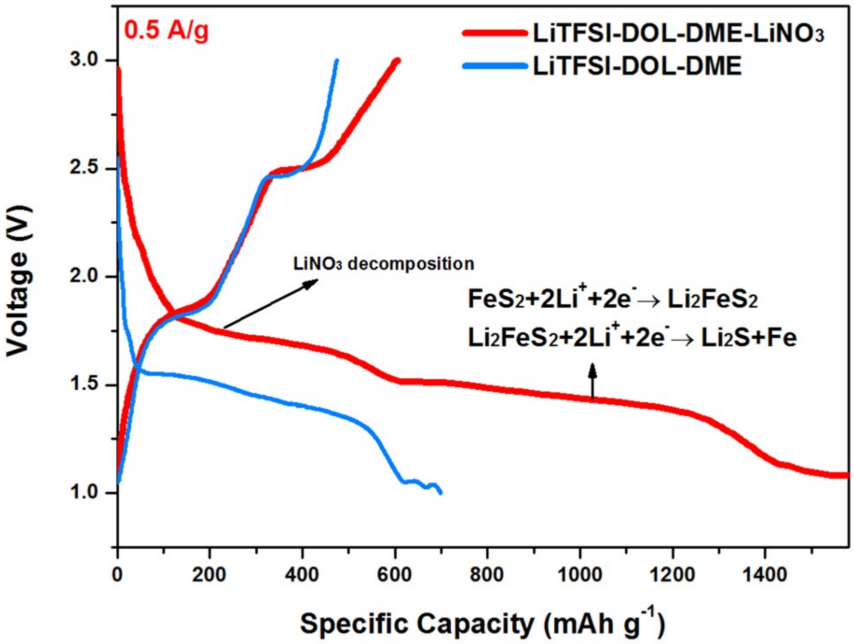

Fig.S7 1st cycle curves of FeS_2@N-graphene at cells with two kinds of electrolytes at 0.5 A g^{-1}.

From the first five CV curves of Li-ion cells without $LiNO_3$ were shown in Fig. S6, a single reduction peak was shown at approximate 1.3 V, attributing to the following reactions[1, 2, 3]:

$$FeS_2 + 2Li^+ + 2e^- \rightarrow Li_2FeS_2 \qquad (1)$$

$$Li_2FeS_2 + 2Li^+ + 2e^- \rightarrow Li_2S + Fe \qquad (2)$$

Around room temperature (~30 °C), these two reactions proceed synchronously due to the slow diffusion of Li-ion into pyrite, explaining the single platform at about ~1.4 V in the **Fig. S7**. From the second cycle onwards, there is a slight change at about 1.99 and 2.20 V reflecting new reactions proceeding. According to the previous studies[4,5], the charging steps may attribute to the following reactions:

$$Li_2S + Fe \rightarrow Li_2FeS_2 + 2Li^+ + 2e^- \qquad (3)$$

$$Li_2FeS_2 \rightarrow Li_{2-x}FeS_2 + xLi^+ + xe^- \quad (0.5 \leq x \leq 0.8) \qquad (4)$$

$$Li_{2-x}FeS_2 \rightarrow FeS_y + (2-y)S + (2-x)Li^+ + (2-x)e^- \quad (0.8 < x \leq 2) \qquad (5)$$

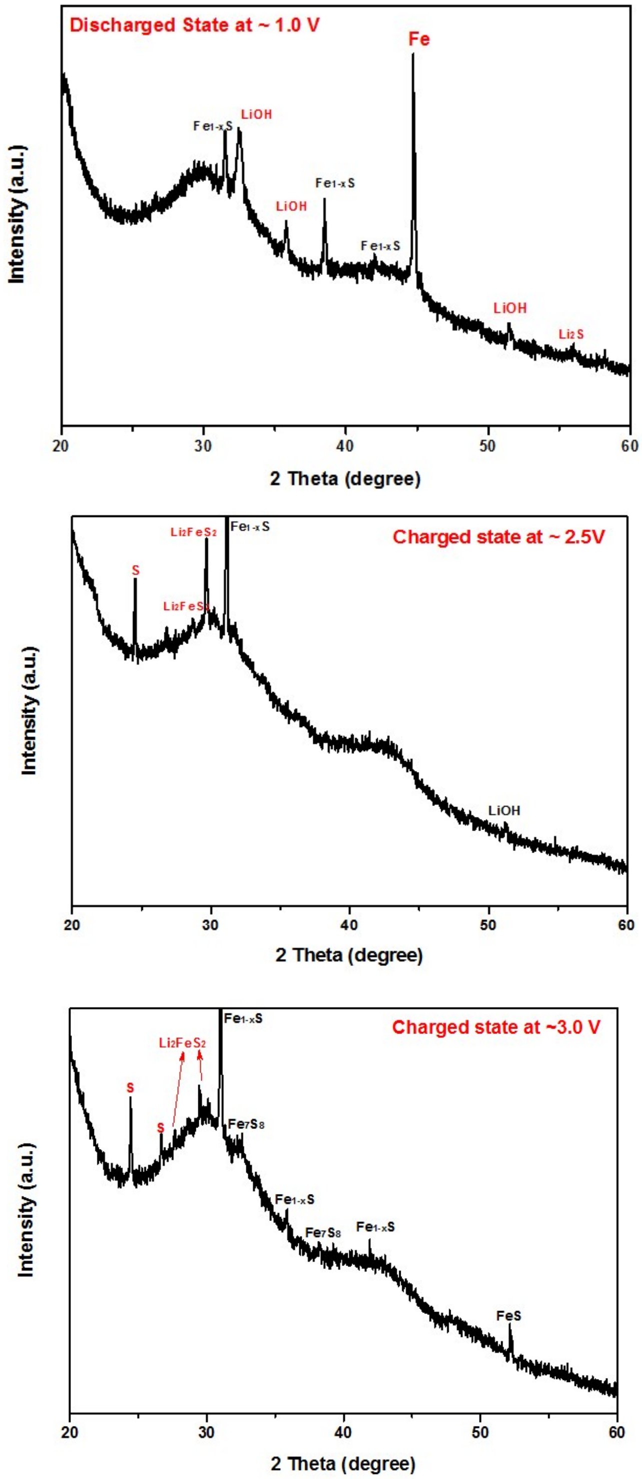

Fig. S8 XRD patterns at different charging-discharging state (~1.0, 2.4, 2.6 V).

When discharged to ~ 1.0 V, the Fe, Li_2S, $Fe_{1-x}S$ and LiOH were found. Due to the cathode plates exposed in the air during the XRD test, most Li_2S were reacted with H_2O to form LiOH and H_2S. As described in the manuscript, Fe and Li_2S were the final discharging products, of which Fe can form a conductive framework contributing to the reversible redox proceeding. Then the batteries were charged to ~

2.5 V, the intermediate product Li_2FeS_2 appeared. With the number of extracted Li^+ in Li_2FeS_2 increased, the structural changes make Li^+ transfer harder from and some part of $(S_2)^{2-}$ starts to lose e^-, resulting into the form of sulfur showing in the XRD patterns of charged state at ~2.5 V. With more Li^+ extracted (charged state at ~3.0 V) , the intermediate product Li_2FeS_2 nearly disappeared. Meanwhile the sulfur and iron-sulfur complexes ($Fe_{1-x}S$, Fe_7S_8 and FeS) were produced. During this procedure, Two kinds of Li^+ in LiS_4 with tetrahedron structure and LiS_6 with octahedron structure, respectively, co- exist in $Li_{2-x}FeS_2$ structure.[6-8] When $0<x<0.8$ in $Li_{2-x}FeS_2$, tetrahedral Li^+ ions start to be extracted and Fe^{2+} changes to Fe^{3+} shown in the State 3.1 of Fig. 3d. During such period, Li^+ and e^- can transfer smoothly due to the stable $Li_{2-x}FeS_2$ structure with LiS_6 octahedron. However, while the content of tetrahedral Li^+ ions decrease to low ratio, S^{2-} oxidation reaction ($S^{2-} \rightarrow 1/2(S_2)^{2-}$) happens and octahedral Li^+ ions transfer increase, directly resulting in the huge volume change of $Li_{2-x}FeS_2$ structure. Li^+ extraction from these intermediate structures are difficult with high polarization due to the low electronic conductivity, which cause that some part of $(S_2)^{2-}$ is overcharged to form sulfur nano-particles shown in State 3.2 of Fig.3d. With the x in $Li_{2-x}FeS_2$ increasing (x from 0 to 1.5) , the Li^+ diffusivity decrease from 5.0×10^{-8} cm s^{-1} to 2×10^{-9} cm s^{-1}.[7]

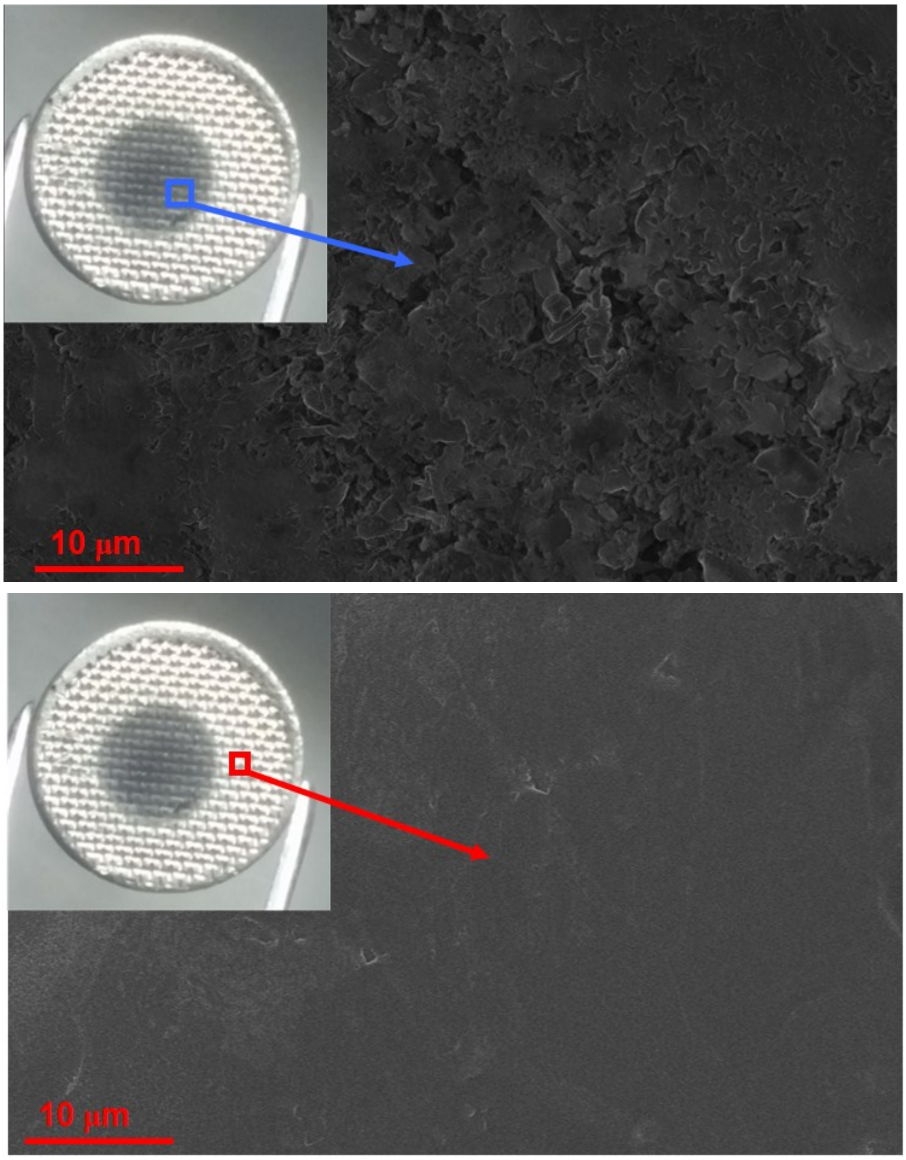

Fig. S9 SEM images of cycled metallic lithium anode.

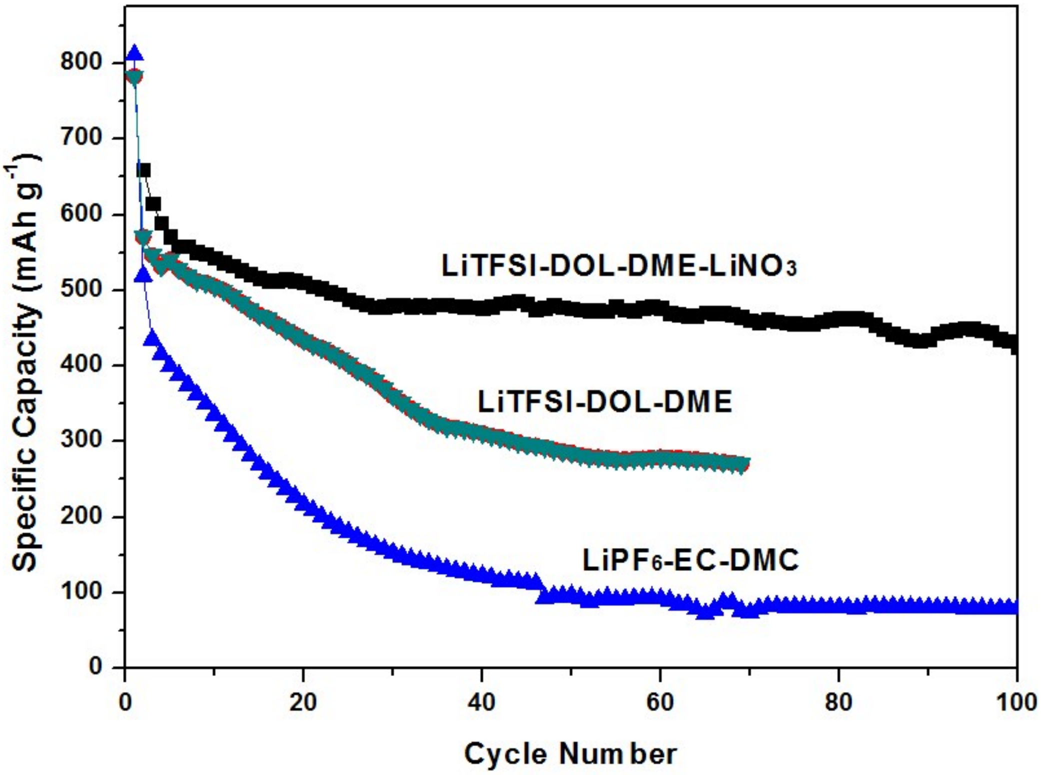

Fig. S10 Cycling performance of nano-FeS_2@N-graphene cathodes in three kinds of electrolytes.

Ether-based electrolyte with $LiNO_3$ is usually applied in Li-S batteries. According to the charging-discharging mechanism of FeS_2 electrodes, Li_2S_x ($2 \leq x \leq 8$) could be formed during the charging-discharging procedure and dissolve in the electrolyte to lead to unfavorable side reactions with lithium metal. DOL and $LiNO_3$ in this electrolyte can protect anodes to stop the “shuttle effect” of immediate sulfur.

The cells with nano-FeS_2@N-graphene cathodes and $LiPF_6$-EC-DMC electrolyte were tested at 0.5 A g^{-1} (**Fig. S10**). The capacities of these cells decay very fast. The reason is because of the intermediate Li_2S_x ($2 \leq x \leq 8$) can react with the carbonate solvent, resulting in irreversible loss of active materials, thus the carbonate-based electrolytes may be inappropriate for use in FeS_2 batteries.

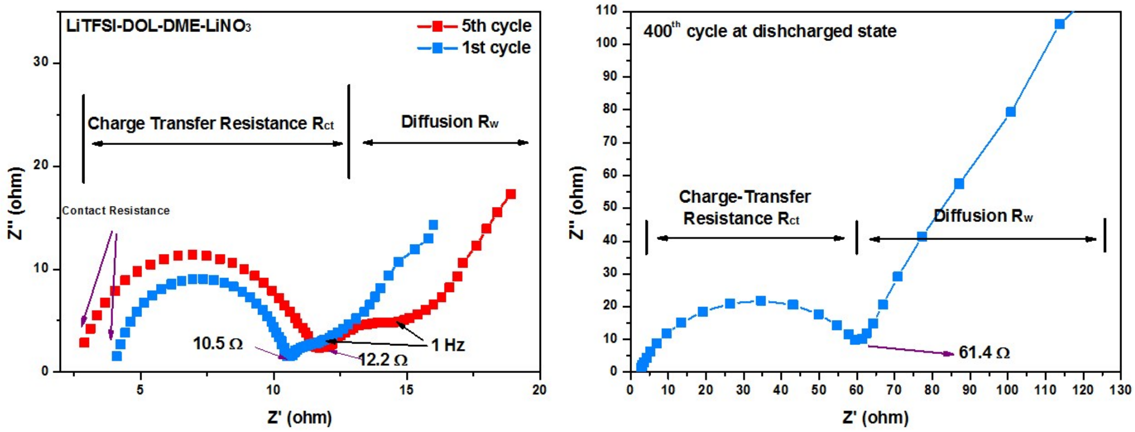

Fig. S11 A-C impediance curves of FeS_2@N-graphene at electrolytes ($LiNO_3$ involved) from 1st to 5th cycle, then to 400th cycle at discharged states.

References

1 T. Evans, D. M. Piper, S. C. Kim, S. S. Han, V. Bhat, K. H. Oh and S. H. Lee, Adv. Mater., 2014, **26**, 7386.

2 J. Liu, Y. Wen, Y. Wang, P. A. van Aken, J. Maier and Y. Yu, Adv. Mater., 2014, **26**, 6025.

3 S.-B. Son, T. A. Yersak, D. M. Piper, S. C. Kim, C. S. Kang, J. S. Cho, S.-S. Suh, Y.-U. Kim, K. H. Oh and S.-H. Lee, Adv. Energy Mater., 2014, 4, 1300961.

4 F. Rosamaria, J.R. Dahn and C. H. W. Jones, J. Electrochem. Soc., 1989, **136**, 3206.

5 A. Le Mehaute and A. Dugast, J. Power sources, 1983, **9**, 359.

6 Z. Wang, C. Wu, L. Liu, J. Electrochem. Soc., 2002, **149**, A466.

7 E. Kendrick, J. Barker, J. Bao, A. Swiatek, J. Power sources, 2011, **196**, 6929;

8 R. Brec, E. Prouzet, G. Ouverard, J. Power Sources, 1989, **26**, 325.